Pyrite formation from FeS and H_2S is mediated by a novel type of microbial energy metabolism

Joana Thiel[1], James Byrne[2], Andreas Kappler[2], Bernhard Schink[1], Michael Pester[1,3]

[1] *University of Konstanz, Universitätsstraße 10, 78464 Konstanz, Germany*

[2] *Eberhardt Karls University of Tübingen, Hölderlinstraße 12, 72074 Tübingen, Germany*

[3] *Leibniz Institute DSMZ – German Culture Collection for Microorganisms and Cell Cultures, Inhoffenstraße 7B, 38124 Braunschweig, Germany*

Short title: Microbial pyrite formation

Keywords: Sulfur cycle | Iron-sulfur minerals | biogenic mineral transformation | syntrophy | deep biosphere | Origin of Life

Corresponding author: Michael Pester

Mail: Michael.Pester@dsmz.de

Phone: +49 531 2616237

Fax: +49 531 2616418

Abstract

The exergonic reaction of FeS with H_2S to form FeS_2 (pyrite) and H_2 was postulated to have operated as an early form of energy metabolism on primordial Earth. Since the Archean, sedimentary pyrite formation played a major role in the global iron and sulfur cycles, with direct impact on the redox chemistry of the atmosphere. To date, pyrite formation was considered a purely geochemical reaction. Here, we present microbial enrichment cultures, which grew with FeS, H_2S, and CO_2 as their sole substrates to produce FeS_2 and CH_4. Cultures grew over periods of three to eight months to cell densities of up to $2–9\times10^6$ cells mL^{-1}. Transformation of FeS with H_2S to FeS_2 was followed by ^{57}Fe Mössbauer spectroscopy and showed a clear biological temperature profile with maximum activity at 28°C and decreasing activities towards 4°C and 60°C. CH_4 was formed concomitantly with FeS_2 and exhibited the same temperature dependence. Addition of either penicillin or 2-bromoethanesulfonate inhibited both FeS_2 and CH_4 production, indicating a syntrophic coupling of pyrite formation to methanogenesis. This hypothesis was supported by a 16S rRNA gene-based phylogenetic analysis, which identified at least one archaeal and five bacterial species. The archaeon was closely related to the hydrogenotrophic methanogen *Methanospirillum stamsii* while the bacteria were most closely related to sulfate-reducing *Deltaproteobacteria*, as well as uncultured *Firmicutes* and *Actinobacteria*. We identified a novel type of microbial metabolism able to conserve energy from FeS transformation to FeS_2, which may serve as a model for a postulated primordial iron-sulfur world.

Significance statement

Pyrite is the most abundant iron-sulfur mineral in sediments. Over geological times, its burial controlled oxygen levels in the atmosphere and sulfate concentrations in seawater. Its formation in sediments is so far considered a purely geochemical process that is at most indirectly supported by microbial activity. We show that lithotrophic microorganisms can directly transform FeS and H_2S to FeS_2 and use this exergonic reaction as a novel form of energy metabolism that is syntrophically coupled to methanogenesis. Our results provide insights into a syntrophic relationship that could sustain part of the deep biosphere and lend support to the iron-sulfur-world theory that postulated FeS transformation to FeS_2 as a key energy-delivering reaction for life to emerge.

Introduction

With an annual formation of at least 5 million tons, pyrite (FeS_2) is the thermodynamically stable end product of iron compounds reacting with sulfide in reduced sediments, with the latter being produced mainly by microbial sulfate reduction. Consequently, pyrite is the most abundant iron-sulfur mineral on Earth's surface (1). Over geological times, burial of pyrite was tightly intertwined with organic matter preservation in reduced sediments (2). These massive reservoirs of reduced sulfur and carbon are being counterbalanced by the photosynthetically produced oxygen in the Earth's atmosphere (2). Despite this importance of pyrite for Earth's iron, sulfur, and carbon cycles as well as Earth's surface redox state, the mechanism of pyrite formation in natural environments is still being debated (1). Currently, two mechanisms are discussed to drive pyrite formation in sediments, which both preclude dissolution of precipitated iron(II) monosulfide (FeS) to an aqueous FeS intermediate. In the polysulfide pathway, FeS_{aq} is attacked by nucleophilic polysulfide to form FeS_2 (equ. 1). Alternatively, pyrite may form from the reaction of FeS_{aq} with H_2S (equ. 2), which is known as the H_2S pathway or the Wächtershäuser reaction (1).

Equ. 1: $FeS + S_n^{2-} \rightarrow FeS_2 + S_{n-1}^{2-}$ $\quad \Delta G_r^{0'} = -64$ to -75 kJ mol^{-1}

Equ. 2: $FeS + H_2S \rightarrow FeS_2 + H_2$ $\quad \Delta G_r^{0'} = -41$ kJ mol^{-1}

Using inorganic experimental systems, abiotic pyrite formation has been observed at temperatures of 25–125°C (e.g. 1, 3). However, already trace amounts of organic compounds containing aldehyde groups were reported to inhibit pyrite formation in such experiments (1, 4). Absence of stringent control for such compounds may explain why many other studies with abiotic systems did not observe pyrite formation at environmentally relevant temperatures (5-

11). On the other hand, pyrite formation is known to take place in the presence of organic matter and especially alive microorganisms in sediments (5, 12). Indeed, pyrite formation could be observed as a side reaction in pure and enrichment cultures of heterotrophic sulfate-reducing and chemolithotrophic sulfur-dismutating bacteria, with the assumption that these microorganisms provide mainly H_2S as a substrate for concomitant abiotic pyrite formation (13-15). In addition, a more complex involvement of microorganisms has been postulated that includes the support of nucleation of FeS minerals on bacterial cell surfaces (16). However, in all these studies biogenic pyrite formation has so far been understood only as an indirect abiotic process.

Pyrite formation according to equ. 2 provides reducing equivalents in the form of H_2 that could be coupled to the reduction of CO_2 to CH_4 or more complex organic matter. Coupling of pyrite formation to methanogenesis has been proposed by Jørgensen and coworkers to be part of a cryptic sulfur cycle in deep marine sediments where it could support the enigmatic life forms of the deep biosphere (17). Coupling of this reaction to the synthesis of organic matter is the basis of the “iron-sulfur world” theory proposed by Wächtershäuser, by which pyrite formation is viewed as the central process that led to the transition from Fe-S surface-catalyzed synthesis of organic molecules to actual life on the primordial Earth (18-20). Here, we show for the first time that the reaction of FeS with H_2S to form FeS_2 can be used by microorganisms to conserve energy for lithotrophic growth if syntrophically coupled to methanogenesis.

Results and Discussion

Pyrite formation as a microbially catalyzed process

Mineral medium containing 5 mM FeS and 6 mM H_2S as sole substrates and CO_2/HCO_3^- as carbon source was inoculated with digested sewage sludge, freshwater or marine sediment (Table S1) and incubated at 16°C or 28°C. Microbial activity was followed via methane formation, and transfers were made every three to eight months, typically when the methane content in the headspace approached a plateau. Of seven enrichments started, four exhibited methane formation for more than ten transfers. The most active enrichment culture J5, which was started from digested sewage sludge and incubated at 28°C, was characterized in more detail after more than 20 transfers. On average, the methane content reached 0.7 mmol per L of culture in J5. In contrast, no methane formation was observed in abiotic controls (Fig. 1*A*). This was mirrored in the turnover of total H_2S: While in culture J5 total H_2S decreased over time from approx. 6 mmol to 0.04–1.1 mmol per L of culture (Fig. S1), abiotic controls showed a much less pronounced decline of total H_2S (3.7 mmol residual H_2S per L). The observed decrease in the abiotic controls may be due to inorganic background reactions (see below).

Conversion of FeS solids was followed by ^{57}Fe Mössbauer spectrometry. After nearly seven months of incubation, the Mössbauer spectrum of culture J5 was dominated by a FeS_2 doublet (Fig. 1*B*), which corresponded to 53–63% of the iron-sulfur mineral phase (Table S2). In contrast, no evidence of a singlet peak corresponding to FeS was present. In addition, a poorly defined sextet feature was required to achieve a satisfactory fit of the Mössbauer spectrum. This poorly defined sextet is best described as a metastable phase, which we have termed FeS_x in accordance with the notation used by Wan et al. (21), and represented 31–39% of the remaining iron-sulfur minerals. Furthermore, a well-defined sextet with a hyperfine magnetic

field of 32 T was required to fit the data, which corresponded well to greigite (Fe_3S_4) (22) and made up 7–8% of the remaining iron-sulfur minerals. Greigite is the sulfur isomorph of magnetite and was previously observed as an intermediate phase in the FeS conversion to pyrite in abiotic studies (23, 24).

FeS_2 formation in culture J5 was confirmed by X-ray diffraction analysis, which recovered all major XRD reflections of pyrite in the obtained XRD pattern (Fig. 2*A*). Since no indication of a parallel formation of the dimorph marcasite was evident from the XRD pattern, the recovered FeS_2 phase is referred to as pyrite from here on. Further support for pyrite formation in culture J5 was provided by scanning electron microscopy (SEM) coupled to energy-dispersive X-ray (EDX) spectroscopy. Here, µm-scale iron-sulfur crystals with a euhedral structure as typical of pyrite could be observed (Fig. 2*B*), which resembled the expected Fe:S ratio of 1:2 as revealed by EDX point measurements (Fig. S2).

In contrast to culture J5, the Mössbauer spectrum of the nearly seven-months-old abiotic control was dominated by a prominent FeS singlet peak (64% of iron-sulfur minerals). In addition, a poorly defined sextet corresponding to FeS_x was required to achieve a satisfactory fit of the obtained data (36% of iron-sulfur minerals) (Fig. 1, Table S2). The abiotic conversion of FeS to FeS_x most likely explains the observed decrease of total H_2S in the abiotic control. Absence of pyrite formation in abiotic controls was further supported by the obtained XRD patterns (Fig. 2*A*). In addition, freshly prepared medium was also devoid of pyrite as evidenced by an overall disordered iron-sulfur mineral phase in SEM-EDX images without any euhedral crystals indicative of pyrite (Fig. 2*B*, Fig. S2).

To further support our hypothesis of biogenic pyrite formation in culture J5, we followed its iron-sulfur mineral transformation over a temperature gradient of 4–60°C. The maximum of pyrite

formation was evident at 28°C. Incubation at lower (16°C) or higher (46°C) temperatures resulted in decreased pyrite formation, with no pyrite formation at 4°C and 60°C (Fig. 3*A* and 3*B*, Table S2). While FeS was completely transformed to pyrite, greigite, and various FeS_x phases at 16, 28, and 46°C, some residual FeS remained at 4°C and 60°C (Fig. 3*A*). The observed temperature profile of pyrite formation is typical of biologically catalyzed reactions centered on an optimum reaction temperature. In contrast, abiotic pyrite formation at temperatures of <100°C was shown to follow a sigmoidal temperature dependence (3).

Microbial pyrite formation is a syntrophically coupled process

Methane formation closely followed the temperature-dependent activity profile of pyrite formation (Fig. 3*C*) suggesting metabolic coupling of both processes. This hypothesis was further explored in an inhibition experiment using either penicillin G as a generic inhibitor of bacterial cell wall synthesis or 2-bromoethanesulfonate (BES) as a specific inhibitor of hydrogenotrophic methanogenesis (25). BES inhibited both methane and pyrite formation completely (Fig. 1*C* and 1*D*). We interpret this as a direct coupling of biogenic pyrite formation to hydrogenotrophic methanogenesis. In support of this hypothesis, penicillin inhibited both pyrite and methane formation as well (Fig. 1*C* and 1*D*). Here, methane formation ceased after an initial production of 0.15 mmol per L of culture. The latter is explained by penicillin's mode of action, which inhibits growth of bacteria but not their initial metabolic activity. Interestingly, a corresponding small amount of pyrite was not observed in this experiment but rather a partial FeS transformation to various FeS_x phases and greigite (Fig. 1*D*, Table S2). This indicates that methanogenesis could receive reducing equivalents also from these iron-sulfur mineral transformations. Further support for syntrophic coupling of pyrite formation to methanogenesis was provided by a third inhibition experiment in which penicillin addition was supplemented by

79% H_2 in the headspace. Also here, pyrite was not formed (Table S2) while methane production was stimulated more than 10-fold by the added H_2 (>10 mmol per L of culture). This clearly showed that methanogenesis could be uncoupled from pyrite formation and is essential for the latter, most likely to keep H_2 or another electron carrier at a low level, to make pyrite formation energetically more favorable as is typically observed in syntrophic processes (26). Although we could not identify the exact electron carrier, molecular H_2 is the most likely candidate because it was previously observed in abiotic experiments of pyrite formation from FeS and H_2S (3, 27). Irrespective of the actual electron carrier, syntrophic coupling of pyrite formation to methanogenesis would be exergonic and result in an expected ratio of formed pyrite to methane of 4:1 (equ. 5).

Equ. 3: $4\ FeS + 4\ H_2S \rightarrow 4\ FeS_2 + 4\ H_2$ ($\Delta G_r^{\circ\prime} = -41$ kJ/mol FeS_2)

Equ. 4: $CO_2 + 4\ H_2 \rightarrow CH_4 + 2\ H_2O$ ($\Delta G_r^{\circ\prime} = -131$ kJ/mol CH_4)

Equ. 5: $4\ FeS + 4\ H_2S + CO_2 \rightarrow 4\ FeS_2 + CH_4 + 2\ H_2O$ ($\Delta G_r^{\circ\prime} = -295$ kJ/mol CH_4)

Indeed, the ratio of pyrite to methane formed in culture J5 was 4.1:1 and 3.2:1 in two independent experiments at 28°C (Table S2), respectively, thus confirming the proposed overall reaction stoichiometry.

Exergonic pyrite formation supports microbial growth

Culture J5 was transferred more than 20 times on medium containing FeS, H_2S and CO_2 as sole substrates. This indicates a strict dependence on syntrophic pyrite formation as the only energy-yielding reaction observed. Within incubation periods of 83–248 days, cell densities increased by more than one order of magnitude, from 2×10^5 cells mL^{-1} to $2–9\times10^6$ cells mL^{-1} (Fig. S3). Cells were typically found to be attached to mineral surfaces (Fig. 4*C*); however,

there was no indication of cell encrustation (Fig. 4*D*). Assuming an average cell volume of about 1 μm^3 and a dry mass content of 33% (28), our measured cell densities correspond to a maximum of ca. 3 mg dry cell mass L^{-1}. If formation of ATP requires 60–70 kJ mol^{-1} (29) and if – under ideal growth conditions – 10.5 g biomass (dry weight) can be synthesized at the expense of 1 mol ATP (30), a complete conversion of 5 mM FeS + 5 mM H_2S according to equ. 5 could yield 4–5 mM ATP or ca. 50 mg dry cell mass L^{-1}. Of course, the conditions of lithoautotrophic growth in our enrichment cultures are entirely different from those used in the growth experiment by Bauchop and Elsden, with heterotrophic growth in an organically rich medium. Moreover, formation of pyrite from FeS is an extremely slow process catalyzed at or close to mineral surfaces with very slow substrate turnover, which implies that major amounts of metabolic energy have to be invested in cell maintenance without concomitant growth (31). Thus, it is not surprising that our cell yields are lower than estimated above. If every partial reaction in equ. 5 (5 in total; 4 × FeS transformation, 1 × CH_4 formation) uses about 20 kJ for synthesis of a minimum of 1/3 of an ATP equivalent (29), the total process could synthesize 5/3 mmol ATP equivalents per liter. Considering that in culture J5 a maximum of 62.5% FeS conversion to FeS_2 was observed (Table S2), the expected cell yield would – optimally – be 12 mg cell dry matter L^{-1}, which is close to the measured cell yield.

The community composition of culture J5 was analyzed by 16S rRNA gene clone libraries. All 16S rRNA gene sequences derived from amplification with a universal archaeal primer set belonged to the same species-level operational taxonomic unit (OTU, 99% sequence identity) and showed 97.6% sequence identity to *Methanospirillum stamsii* (Fig. 4*B*), a hydrogenotrophic methanogen isolated from a low-temperature bioreactor (32). Methanogenesis in culture J5 is likely performed by this OTU. Using a universal bacterial

primer set, we detected five bacterial OTUs (Fig. 4*A*). The majority of clones (76%) belonged to OTU 3, which showed 99.9% sequence identity with *Desulfomicrobium baculatum*, a sulfate reducer within the class Deltaproteobacteria (33, 34). Further OTUs related to Deltaproteobacteria were OTU 2 (12% rel. abundance) and OTU1 (6% rel. abundance). OTU 2 was closely related to *Desulfovibrio sulfodismutans* (97.9% sequence identity), which is capable of dismutating thiosulfate or sulfite (35), while OTU 1 was distantly related (96.2% sequence identity) to *Smithella propionica,* which is known to degrade propionate in syntrophy with methanogens (36). The remaining two bacterial OTUs were either distantly related (<91% sequence identity) to cultured members of the Firmicutes (OTU 4, 3% rel. abundance) or Actinobacteria (OTU 5, 3% rel. abundance). Interestingly, all OTUs belonging to the Deltaproteobacteria and Firmicutes fell into larger clusters that include cultured representatives with a sulfur-related energy metabolism. Therefore, it is tempting to speculate that enzymes operating in the respective sulfur transformation pathways might be involved in the microbial conversion of FeS to FeS_2.

Conclusion

Pyrite is produced in massive quantities in today's sediments (2). However, its formation in nature is far from understood, especially because its nucleation is kinetically hindered (1). The presence of sulfide-producing microorganisms as passive pyrite nucleation sites indicated support for abiotic pyrite formation (13-15), but could not be reproduced in every bacterial model system (6). We show that pyrite formation can be mediated by microorganisms to overcome the kinetic hurdle of nucleation, but as an essential part of their energy metabolism and not just as a mere abiotic side reaction on their cell surface. This may help to explain the ambiguous results published so far on the role of microorganisms in this process. Since we

found only one archaeal species closely related to methanogens in our enrichments, it is likely that one or several of the bacterial partners actually catalyze FeS transformation to pyrite. An exciting question currently remaining is whether these bacteria utilize internally the H_2S pathway (equ. 2) or a combination of sulfide oxidation to zero-valent sulfur coupled to the polysulfide pathway (equ. 1) to finally produce pyrite (Fig. S4).

Our results further showed that the reducing equivalents released from FeS transformation to pyrite can be transferred to methanogenesis. This opens an interesting perspective on the metabolic versatility sustaining the vast deep biosphere inhabiting the Earth's subsurface (37). While recalcitrant organic matter or H_2 released by radiolytic cleavage of water (38, 39) have been proposed to sustain the enigmatic life forms of the deep biosphere, there is also experimental evidence of a cryptic sulfur cycle within deep sediments that would include pyrite formation coupled to methanogenesis to be functional (17). Our results show that this missing link could indeed be mediated by microorganisms and supply energy to support microbial growth. Since the redox potential ($E_h°'$) of the FeS/FeS_2 couple is –620 mV at circumneutral pH (40), it is well suited to provide reducing equivalents also for CO_2 fixation to acetate ($E_h°'$ = –290 mV) and more complex organic matter in the pyrite-forming microorganism. Wächtershäuser proposed in his "iron-sulfur world" theory that exactly this mechanism was the basis for an autocatalytic metabolism and the resulting evolution of life at hydrothermal vents on primordial Earth (e.g. 20, 41). Our enrichment cultures may serve as a model to understand the enzymatic background of this hypothesis.

Methods

Cultivation

Enrichment cultures were initiated and maintained in carbonate-buffered, sulfide-reduced (1 mM) freshwater mineral medium (42) supplemented with selenite-tungstate solution (43), 7-vitamin solution (42), and trace element solution SL10 (44). The medium was prepared and stored under a N_2/CO_2 atmosphere (80:20). The final pH was adjusted to 7.2 to 7.4. From a CO_2-neutralized sulfide stock solution (45), 350 µmol H_2S was added to 70 mL mineral medium in 180 mL serum bottles that were sealed with butyl rubber stoppers. Since 1 mM H_2S was already present as reducing agent in the mineral medium, the final amount of H_2S was 420 µmol. FeS was prepared from anoxic solutions of 0.4 M $FeCl_2$ and 0.4 M Na_2S. The resulting FeS precipitate was washed at least once and re-suspended in oxygen-free distilled water. For Mössbauer spectroscopy analysis, FeS was prepared from a $FeCl_2$ solution that contained 10% $^{57}FeCl_2$ to enhance signal quality. 350 µmol FeS was added to 70 mL mineral medium. Enrichment cultures were incubated in the dark at 28°C if not indicated otherwise. For inhibition experiments, cultures were supplemented with either penicillin-G (1,000 U mL^{-1}) or 2-bromoethanesulfonate (10 mM). Abiotic controls were run without inoculum.

Monitoring of substrate turnover

For total dissolved sulfide measurements [$\Sigma(H_2S_{aq}, HS^-, S^{2-})$], 100-µL samples were taken from liquid cultures without disturbing the precipitated iron sulfide minerals, and directly transferred to 100 µL of an anoxic 0.2 M NaOH solution. From the alkalinized sample, 10–20 µL were fixed in 100 µL of a 0.1 M zinc acetate solution, and sulfide was quantified by the methylene blue method (46). The corresponding amount of H_2S in the headspace was calculated using Henry's law and a temperature-adjusted k-value of 0.093 (28°C, 47). CH_4 was

measured by gas chromatography with a flame ionization detector (SRI Instrument SGI 8610C) using a consecutive arrangement of a Porapak (80/100 mesh; 1 m × 2 mm) and a Hayesep-D packed column (80/100 mesh; 3 m × 2 mm). The injector and column temperatures were 60°C, and the detector temperature was 135°C. The carrier gas was N_2 at a flow rate of 3.2 ml min^{-1}. Chromatograms were recorded with the PeakSimple v4.44 chromatography software.

Iron-sulfide minerals were analyzed by ^{57}Fe Mössbauer spectroscopy. Within an anoxic glovebox (100% N_2), the enrichment culture was passed through a 0.44-µm filter and then sealed between two pieces of air-tight Kapton tape. Samples were transferred to a Mössbauer spectrometer (WissEl, Starnberg) within an airtight bottle filled with 100% N_2 that was only opened immediately prior to loading the samples inside the closed-cycle exchange gas cryostat (Janis cryogenics). Measurements were collected at a temperature of 5 K with a constant acceleration drive system (WissEL) in transmission mode with a ^{57}Co/Rh source and calibrated against a 7 µm thick α-^{57}Fe foil measured at room temperature. All spectra were analyzed using Recoil (University of Ottawa) by applying the Voight Based Fitting (VBF) routine (48). The half width at half maximum (HWHM) was fixed to a value of 0.138 mm s^{-1} for all samples.

X-ray diffraction (XRD) patterns were recorded with the D8 Discover system (Bruker) with IµS radiation source (2 mm in diameter), and a Lynxexe XE detector. Samples were dried for 2 h under a continuous stream of 100% N_2 and measured within 48 h under air as described previously (49). Measurements were done using CuKα rays in angles ranging from 10–70° 2Θ in 0.02° steps with 2,880 sec measuring time and a total measuring time of 12 h and 47 min. The resulting spectra were compared with spectra provided in the international crystal structure

296 database (ICSD), FIZ Karlsruhe (version 2016/2) using the software DIFFRAC.EVA (version
297 4.1.1, Bruker).

298 ## Scanning electron microscopy coupled to energy dispersive x-ray spectroscopy (SEM-EDX)

299 For SEM-EDX analysis, 1 mL of culture was centrifuged at 4,500 ×*g* for 10 min. 200 µL of the
300 resulting pellet was transferred on gelatin-coated glass slides. Samples were fixed in 1 mL
301 2.5% glutaraldehyde in 0.1 M HEPES-buffer containing 0.01 M KCl (HEPES-KCl) and in 2%
302 OsO_4 in HEPES-KCl for 60 min each. Fixed samples were dehydrated in a graded ethanol
303 series (30%, 50%, 70%, 80%, 90%, 96% and absolute ethanol) for 30 min each. Thereafter,
304 samples were critical-point dried under CO_2 in a Bal-Tec CPD030 (Balzers). Sputter coating of
305 6 nm platinum was done in a Quorum Q150R ES sputter coater (Quorum Technologies) and
306 micrographs were taken with a FESEM Auriga 40 (Zeiss). EDX mappings and point
307 measurements were taken at a working distance of 5 mm with an Oxford X-Max detector
308 (Oxford Instruments) and at 10 kV and 15 kV, respectively. Point measurements were
309 normalized to 10,000 counts within a Kα energy of 6.3–6.5 keV. Sample preparation for cell
310 counts by fluorescent microscopy is described in detail in the Supporting Information.

311 ## Phylogenetic analysis

312 Total genomic DNA was extracted from 50 mL of a 4.5-months old culture using a phenol-
313 based beat-beating protocol modified after Loy, Beisker and Meier (50). Subsequent
314 amplification of bacterial or archaeal 16S rRNA genes was done using standard PCR protocols
315 based on universal primers. Details are given in the Supporting Information. 16S rRNA gene
316 clone libraries were constructed using the TOPO® TA Cloning® Kit (ThermoFisher Scientific).
317 Bacterial or archaeal 16S rRNA gene fragments were aligned by use of the SINA webaligner
318 (51) to the non-redundant 16S rRNA gene database v.123.1 available on the SILVA online

platform (52, www.arb-silva.de) and imported into ARB for initial phylogenetic analysis (53). OTU clustering was performed in mothur v.1.22.2 (54) using the furthest neighbor approach and a 99%-identity cutoff to delineate OTUs at the approximate species level (55). For phylogenetic inference of 16S rRNA gene fragments representing individual OTUs, Maximum Likelihood (ML) trees were calculated using RAxML v8.2.9 (56) as implemented on the CIPRES webserver (57, www.phylo.org). Using a 50% conservation filter of nucleic acid positions within the domain Bacteria, a RAxML tree was inferred from 1,102 unambiguously aligned nucleic acid positions for bacterial 16S rRNA genes. The reconstruction of the archaeal tree followed the same outline but using 752 unambiguously aligned nucleic acid positions and no conservation filter because of the close relatedness of all included sequences. Calculations were based on the GTRGAMMA distribution model of substitution rate heterogeneity. MRE-based bootstrap analysis stopped after 204 and 102 replicates for the bacterial and archaeal 16S rRNA gene tree, respectively. Sequences are available from NCBI GenBank under accession numbers MH665848–MH665880 and MH665881–MH665889 for Bacteria and Archaea, respectively.

Acknowledgements

This study was financed by the Konstanz Research School Chemical Biology (KoRs-CB). We are grateful to Waltraud Dilling for maintaining initial pyrite-forming enrichments and to Ben Griffin for his initial work on the latter. We further thank Michael Laumann for his engagement with SEM-EDX, Stephan Siroky and the Particle Analysis Center for the XRD analysis, as well as the Bioimaging Center (University of Konstanz).

Figures

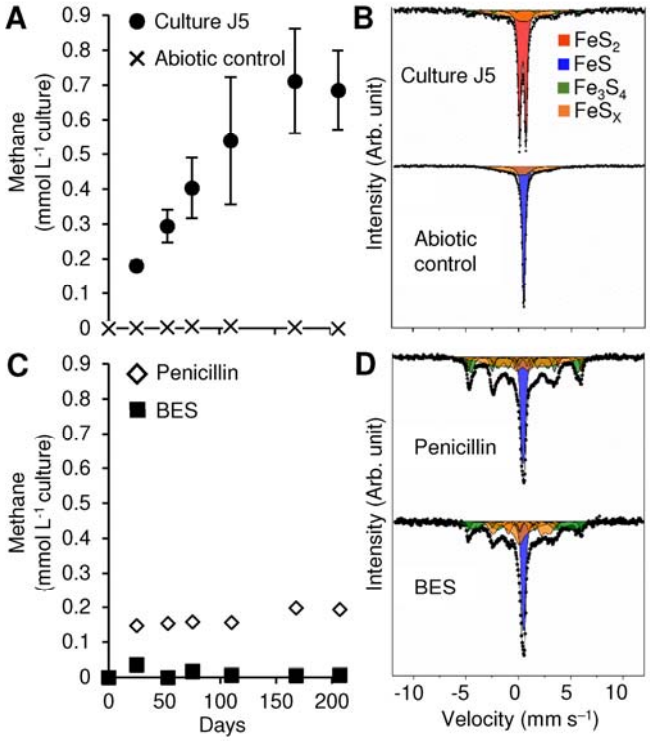

Figure 1. Time-resolved CH_4 formation in comparison to iron-sulfur mineral composition after nearly seven months of incubation (207 days) in culture J5 as compared to abiotic controls and incubations of culture J5 with penicillin-G (1,000 U ml^{-1}) or 2-bromoethanesulfonate (BES, 10 mM). (A) and (C) show the mean ± one standard deviation of CH_4 measurements of three independent incubations. Standard deviations are often smaller than the actual symbol size. (B) and (D) show Mössbauer spectra corresponding to the last time point in the presented time series with FeS_2 in red, FeS in blue, Fe_3S_4 in green, and intermediate FeS_x phases in orange.

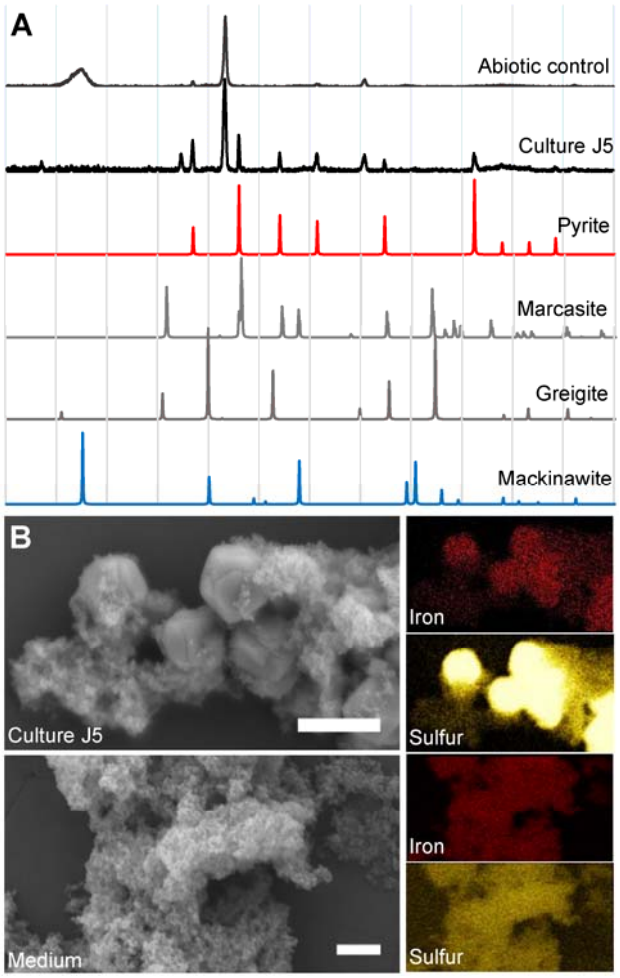

Figure 2. (A) Representative X-ray diffractograms of mineral precipitates formed in culture J5 and an abiotic control setup after 9 months of incubation (281 days). Diffraction data of the two FeS_2 dimorphs pyrite and marcasite as well as of Fe_3S_4 (greigite) and FeS (mackinawite) are given as reference. (B) Scanning electron microscopy images of a nearly 7-months old (211 days) culture J5 in comparison to freshly prepared medium without inoculum. The scale bar represents 2 µm. Images to the right show the corresponding results from energy dispersive X-ray spectroscopy (EDX). Besides atoms from medium salts, iron and sulfur were the only elements discovered in the mineral phases.

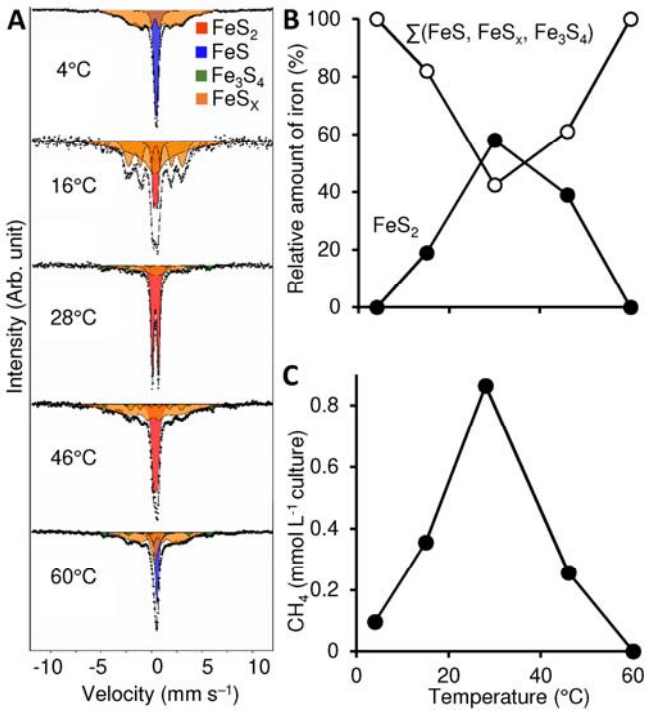

Figure 3. Temperature-dependent pyrite and methane formation in culture J5 after nearly 7 months of incubation (207 days). A) Mössbauer spectra showing the temperature-dependent iron-sulfur mineral composition (FeS_2 in red, FeS in blue, Fe_3S_4 in green, and intermediate FeS_x phases in orange). B) Relative abundance of pyrite (FeS_2) in comparison to all other measured iron-sulfur minerals plotted against temperature as the explanatory variable. Details are provided in Table S2. C) Average amount of methane (n=2) plotted against temperature as the explanatory variable.

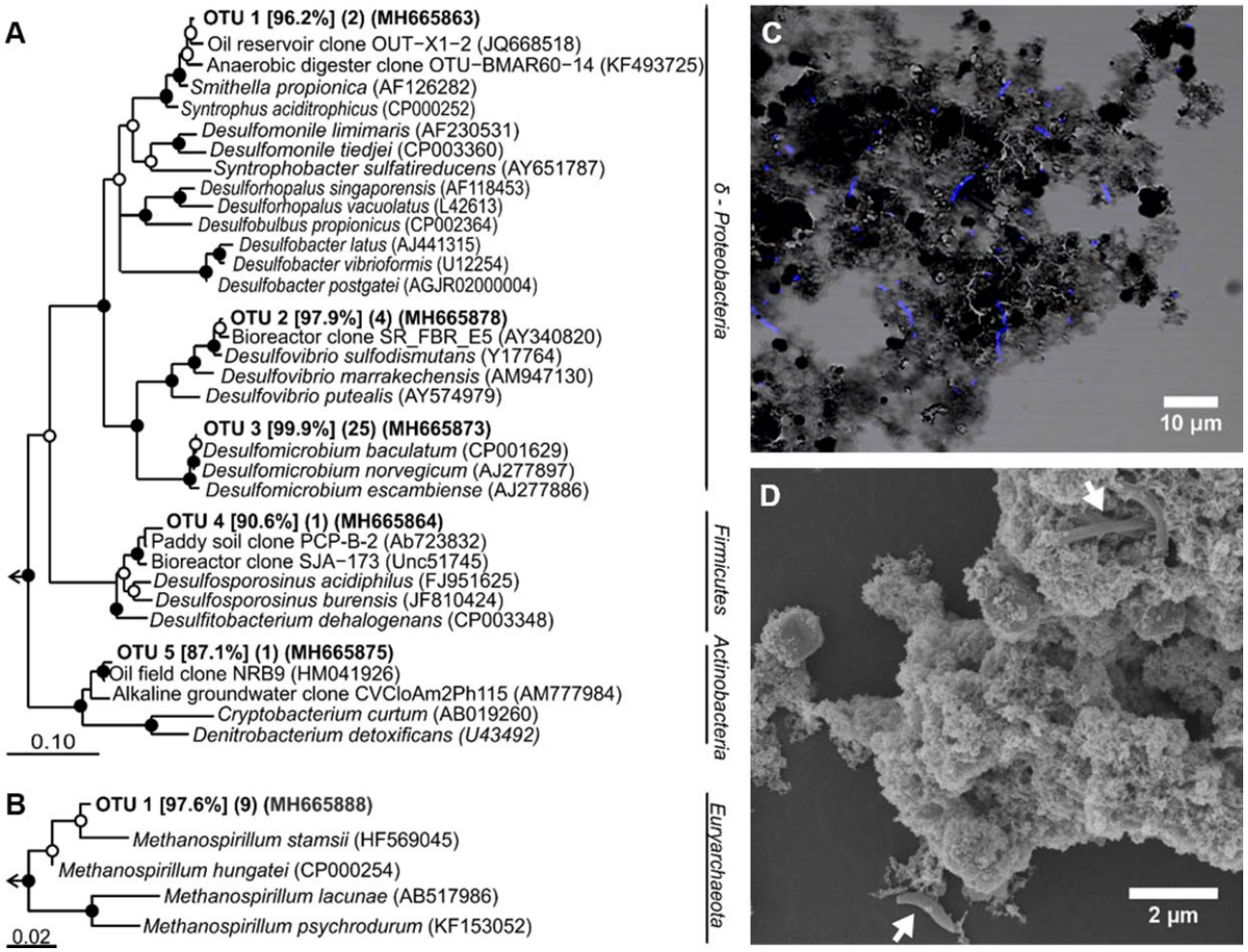

Figure 4. Bacterial and archaeal community composition of enrichment culture J5. RAxML trees based on bacterial (A) and archaeal (B) 16S rRNA gene sequences obtained from culture J5. Representative sequences of OTUs at the approximate species level (99% sequence identity) are shown. Sequence identity to the next cultured relative is given in percent in square brackets. Numbers of clones from the same OTU are presented in parenthesis followed by the GenBank accession number of a representative sequence. Bootstrap support is indicated by closed (≥90%) and open (≥70%) circles at the respective branching points. The scale bar represents 10% (Bacteria) and 2% (Archaea) estimated sequence divergence. (C) Combined phase contrast image and fluorescent image of DAPI-stained cells and (D) scanning electron

376 microscopy image with cells indicated by white arrows of culture J5 after 7.4 and 10 months of

377 incubation, respectively.

378

References

1. Rickard D, Luther GW (2007) Chemistry of iron sulfides. *Chem Rev* 107(2):514-562.

2. Canfield DE, Farquhar J (2012) The global sulfur cycle. *Fundamentals of Geobiology*, eds Knoll H, Canfield DE, & Konhauser KO (John Wiley & Sons, Oxford), pp 49-64.

3. Rickard D, Luther GW (1997) Kinetics of pyrite formation by the H_2S oxidation of iron(II) monosulfide in aqueous solutions between 25 and 125°C: The mechanism. *Geochim Cosmochim Acta* 61(1):135-147.

4. Rickard D, Butler IB, Oldroyd A (2001) A novel iron sulphide mineral switch and its implications for Earth and planetary science. *Earth Planet Sc Lett* 189(1-2):85-91.

5. Berner RA (1970) Sedimentary pyrite formation. *Am J Sci* 268(1):1-23.

6. Picard A, Gartman A, Clarke DR, Girguis PR (2018) Sulfate-reducing bacteria influence the nucleation and growth of mackinawite and greigite. *Geochim Cosmochim Acta* 220:367-384.

7. Wilkin RT, Barnes HL (1996) Pyrite formation by reactions of iron monosulfides with dissolved inorganic and organic sulfur species. *Geochim Cosmochim Acta* 60(21):4167-4179.

8. Schoonen MAA, Barnes HL (1991) Reactions forming pyrite and marcasite from solution .1. Nucleation of FeS_2 below 100°C. *Geochim Cosmochim Acta* 55(6):1495-1504.

9. Rickard D (1969) The microbiological formation of iron sulphides. *Stockholm Contributions to Geology* 20:49-66.

10. Benning LG, Wilkin RT, Barnes HL (2000) Reaction pathways in the Fe-S system below 100°C. *Chem Geol* 167(1-2):25-51.

11. Benning L, Barnes H (1998) In situ determination of the stability of iron monosulphides and kinetics of pyrite formation. *Mineral Mag A* 62:151-152.

12. Berner RA (1984) Sedimentary pyrite formation - an update. *Geochim Cosmochim Acta* 48(4):605-615.

13. Finster K, Liesack W, Thamdrup B (1998) Elemental sulfur and thiosulfate disproportionation by *Desulfocapsa sulfoexigens* sp. nov., a new anaerobic bacterium isolated from marine surface sediment. *Appl Environ Microbiol* 64(1):119-125.

14. Canfield DE, Thamdrup B, Fleischer S (1998) Isotope fractionation and sulfur metabolism by pure and enrichment cultures of elemental sulfur-disproportionating Bacteria. *Limnol Oceanogr* 43(2):253-264.

15. Thamdrup B, Finster K, Hansen JW, Bak F (1993) Bacterial disproportionation of elemental sulfur coupled to chemical-reduction of iron or manganese. *Appl Environ Microbiol* 59(1):101-108.

16. Donald R, Southam G (1999) Low temperature anaerobic bacterial diagenesis of ferrous monosulfide to pyrite. *Geochim Cosmochim Acta* 63(13-14):2019-2023.

17. Holmkvist L, Ferdelman TG, Jørgensen BB (2011) A cryptic sulfur cycle driven by iron in the methane zone of marine sediment (Aarhus Bay, Denmark). *Geochim Cosmochim Acta* 75(12):3581-3599.

18. Wächtershäuser G (1988) Before enzymes and templates: theory of surface metabolism. *Microbiol Rev* 52(4):452-484.

19. Wächtershäuser G (2007) On the chemistry and evolution of the pioneer organism. *Chem Biodivers* 4(4):584-602.

20. Martin W, Russell MJ (2003) On the origins of cells: a hypothesis for the evolutionary transitions from abiotic geochemistry to chemoautotrophic prokaryotes, and from prokaryotes to nucleated cells. *Philos Trans R Soc Lond B Biol Sci* 358(1429):59-83.

21. Wan M, Schroder C, Peiffer S (2017) Fe(III): S(-II) concentration ratio controls the pathway and the kinetics of pyrite formation during sulfidation of ferric hydroxides. *Geochim Cosmochim Acta* 217:334-348.

22. Vandenberghe RE, de Grave E, de Bakker PMA, Krs M, Hus JJ (1992) Mössbauer effect study of natural greigite. *Hyperfine Interact* 68(1):319-322.

23. Hunger S, Benning LG (2007) Greigite: a true intermediate on the polysulfide pathway to pyrite. *Geochem T* 8:1. https://doi.org/10.1186/1467-4866-1188-1181.

24. Bourdoiseau JA, Jeannin M, Remazeilles C, Sabota R, Refait P (2011) The transformation of mackinawite into greigite studied by Raman spectroscopy. *J Raman Spectrosc* 42(3):496-504.

25. Oremland RS, Capone DG (1988) Use of specific inhibitors in biogeochemistry and microbial ecology. *Adv Microb Ecol* 10:285-383.

26. Schink B, Stams AJM (2006) Syntrophism among prokaryotes. *The Prokaryotes*, ed Dworkin M, Falkow, S., Rosenberg, E., Schleifer, K.-H., Stackebrandt, E. (Springer, Singapore), Third Ed Vol 2, pp 309-335.

27. Drobner E, Huber H, Wächtershäuser G, Rose D, Stetter KO (1990) Pyrite formation linked with hydrogen evolution under anaerobic conditions. *Nature* 346(6286):742-744.

28. Bratbak G, Dundas I (1984) Bacterial dry-matter content and biomass estimations. *Appl Environ Microbiol* 48(4):755-757.

29. Schink B (1997) Energetics of syntrophic cooperation in methanogenic degradation. *Microbiol Mol Biol Rev* 61(2):262-280.

30. Bauchop T, Elsden SR (1960) The growth of micro-organisms in relation to their energy supply. *J Gen Microbiol* 23(3):457-469.

31. Pirt SJ (1982) Maintenance energy - a general-model for energy-limited and energy-sufficient growth. *Arch Microbiol* 133(4):300-302.

442 32. Parshina SN, Ermakova AV, Bomberg M, Detkova EN (2014) *Methanospirillum stamsii* sp nov., a
443 psychrotolerant, hydrogenotrophic, methanogenic archaeon isolated from an anaerobic expanded
444 granular sludge bed bioreactor operated at low temperature. *Int J Syst Evol Microbiol* 64(1):180-186.

445 33. Rozanova EP, Nazina TN (1976) A mesophilic, sulfate-reducing, rod-shaped, non-spore-forming
446 bacterium. *Microbiologiya (USSR)* 45(5):825-830.

447 34. Rozanova EP, Nazina TN, Galushko AS (1988) Isolation of a new genus of sulfate-reducing bacteria and
448 description of a new species of this genus, *Desulfomicrobium apsheronum* gen. nov., sp.nov.
449 *Microbiologiya (USSR)* 57(4):634-641.

450 35. Bak F, Pfennig N (1987) Chemolithotrophic growth of *Desulfovibrio sulfodismutans* sp. nov. by
451 disproportionation of inorganic sulfur-compounds. *Arch Microbiol* 147(2):184-189.

452 36. Liu YT, Balkwill DL, Aldrich HC, Drake GR, Boone DR (1999) Characterization of the anaerobic propioate-
453 degrading syntrophs *Smithella propionica* gen. nov., sp. nov. and *Syntrophobacter wolinii*. *Int J Syst*
454 *Bacteriol* 49:545-556.

455 37. Jørgensen BB, Marshall IPG (2016) Slow microbial life in the seabed. *Annu Rev Mar Sci* 8:311-332.

456 38. Jørgensen BB, D'Hondt S (2006) A starving majority deep beneath the seafloor. *Science* 314(5801):932-
457 934.

458 39. Lin L-H, Slater G, Lollar B, Lacrampe-Couloume G, Onstott TC (2005) The yield and isotopic composition
459 of radiolytic H_2, a potential energy source for the deep subsurface biosphere. *Geochim Cosmochim Acta*
460 69(4):893-903.

461 40. Kaschke M, Russell MJ, Cole WJ (1994) [Fes/Fes(2)] - a redox system for the origin of life. *Origins Life Evol*
462 *B* 24(1):43-56.

463 41. Wächtershäuser G (2006) From volcanic origins of chemoautotrophic life to Bacteria, Archaea and
464 Eukarya. *Philos Trans R Soc Lond B Biol Sci* 361(1474):1787-1806.

465 42. Widdel F, Pfennig N (1981) Studies on dissimilatory sulfate-reducing bacteria that decompose fatty
466 acids. I. Isolation of new sulfate-reducing bacteria enriched with acetate from saline environments.
467 Description of *Desulfobacter postgatei* gen. nov., sp. nov. *Arch Microbiol* 129(5):395-400.

468 43. Tschech A, Pfennig N (1984) Growth-yield increase linked to caffeate reduction in *Acetobacterium*
469 *woodii*. *Arch Microbiol* 137(2):163-167.

470 44. Widdel F, Kohring GW, Mayer F (1983) Studies on dissimilatory sulfate-reducing bacteria that
471 decompose fatty-acids .3. Characterization of the filamentous gliding *Desulfonema limicola* gen. nov sp.
472 nov, and *Desulfonema magnum* sp. nov. *Arch Microbiol* 134(4):286-294.

473 45. Siefert E, Pfennig N (1984) Convenient method to prepare neutral sulfide solution for cultivation of
474 phototrophic sulfur bacteria. *Arch Microbiol* 139(1):100-101.

475 46. Cline JD (1969) Spectrophotometric determination of hydrogen sulfide in natural waters. *Limnol*
476 *Oceanogr* 14(3):454-458.

47. Carroll JJ, Mather AE (1989) The solubility of hydrogen-sulfide in water from 0°C to 90°C and pressures to 1 MPa. *Geochim Cosmochim Acta* 53(6):1163-1170.

48. Rancourt DG, Ping JY (1991) Voigt-based methods for arbitrary-shape static hyperfine parameter distributions in mössbauer spectroscopy. *Nucl Instrum Meth B* 58(1):85-97.

49. Taylor P, Rummery TE, Owen DG (1979) Reactions of iron monosulfide solids with aqueous hydrogen-sulfide up to 160°C. *J Inorg Nucl Chem* 41(12):1683-1687.

50. Loy A, Beisker W, Meier H (2005) Diversity of bacteria growing in natural mineral water after bottling. *Appl Environ Microbiol* 71(7):3624-3632.

51. Pruesse E*, et al.* (2007) SILVA: a comprehensive online resource for quality checked and aligned ribosomal RNA sequence data compatible with ARB. *Nucleic Acids Res* 35(21):7188-7196.

52. Quast C*, et al.* (2013) The SILVA ribosomal RNA gene database project: improved data processing and web-based tools. *Nucleic Acids Res* 41(D1):D590-D596.

53. Ludwig W*, et al.* (2004) ARB: a software environment for sequence data. *Nucleic Acids Res* 32(4):1363-1371.

54. Schloss PD*, et al.* (2009) Introducing mothur: open-source, platform-independent, community-supported software for describing and comparing microbial communities. *Appl Environ Microbiol* 75(23):7537-7541.

55. Stackebrandt E, Ebers J (2006) Taxonomic parameters revisited: tarnished gold standards. *Microbiology Today* 33(4):152–154.

56. Stamatakis A (2014) RAxML version 8: a tool for phylogenetic analysis and post-analysis of large phylogenies. *Bioinformatics* 30(9):1312-1313.

57. Miller MA, Pfeiffer W, Schwartz T (2010) Creating the CIPRES Science Gateway for inference of large phylogenetic trees. *2010 Gateway Computing Environments Workshop (GCE)*, pp 1-8.

58. Berthold MR*, et al.* (2008) KNIME: The Konstanz Information Miner. (Springer), pp 319-326.

59. Loy A*, et al.* (2002) Oligonucleotide microarray for 16S rRNA gene-based detection of all recognized lineages of sulfate-reducing prokaryotes in the environment. *Appl Environ Microbiol* 68(10):5064-5081.

60. Berry D, Ben Mahfoudh K, Wagner M, Loy A (2011) Barcoded primers used in multiplex amplicon pyrosequencing bias amplification. *Appl Environ Microbiol* 77(21):7846-7849.

61. Lueders T, Friedrich MW (2002) Effects of amendment with ferrihydrite and gypsum on the structure and activity of methanogenic populations in rice field soil. *Appl Environ Microbiol* 68(5):2484-2494.

62. Casamayor EO*, et al.* (2002) Changes in archaeal, bacterial and eukaryal assemblages along a salinity gradient by comparison of genetic fingerprinting methods in a multipond solar saltern. *Environ Microbiol* 4(6):338-348.

Supporting Information

Supporting Materials and Methods

Cell counts by fluorescence microscopy. For cell counts, 0.5 mL culture was fixed overnight in 9.5 mL freshly prepared paraformaldehyde solution (4%), subsequently centrifuged at 10,000 ×*g* for 10 min at 4°C and re-suspended in 1 mL PBS [130 mM NaCl, 5% (v/v) phosphate buffer (40 mM NaH_2PO_4, 160 mM Na_2HPO_4), pH 7.2] and 9 mL ammonium oxalate solution (5.6 g ammonium-oxalate and 4.2 g oxalic acid dihydrate in 200 mL distilled water). Samples were vortexed for 10 min to dissolve most of the iron sulfide minerals so that cells could be collected on a 0.2 µm pore size filter (GTTP-white, Millipore). Filters were air-dried and stored at –20°C. Filter sections were stained with a 1 µg mL^{-1} 4',6-diamidino-2-phenylindole (DAPI) solution and incubated for 10 min in the dark. Thereafter, filters were washed for 5 min in distilled water, followed by two 1-min washing steps in 80% ethanol. Dry DAPI-stained filters were mounted on microscope slides using CitiFluor™ AF1. For fluorescence microscopy, an inverted microscope (AxioObserver, Zeiss) with a 40x/0.60 LD-PlanNeofluar objective was used. Z-stacks were acquired with a distance of 0.28 µm. Image processing involved 3-dimensional deconvolution of each stack using a theoretical PSF with ZEN Black (Zeiss AG). Cells were counted using an image processing workflow set up in KNIME 3.4.0 (58) using orthogonal projections of the de-convoluted input stacks. The workflow is available at https://github.com/bic-kn/cell-counting-workflow.

DNA extraction. The DNA extraction protocol was adopted from (50). A 4.5-month old 50-mL culture was harvested after CH_4 concentrations reached a plateau of 2.1% in the headspace (corresponding to 55 µmol produced CH_4). Harvesting was done by 10 min of centrifugation at 6,000 ×*g*. The pellet was re-suspended in 400 µL autoclaved TE-Buffer (10 mM Tris & 1 mM

533 EDTA in MQ water, pH 8) and stored for three hours at –20°C. Cells were thawed on ice,
534 mixed with heat-sterilized zirconium beads (0.1 mm), 600 µL phenol/chloroform/isoamylalcohol
535 (25:24:1, Carl Roth), and 150 µL of a 10% sterile-filtered SDS-solution in a screw-cap tube,
536 and vigorously shaken for 20 min using a vortexer. After centrifugation for 20 min at 20,817 ×*g*
537 and 4°C, the aqueous supernatant was transferred to a new reaction tube. Because the
538 aqueous phase was hardly visible due to remaining iron sulfide minerals, another 10-minute
539 centrifugation step was used to remove residual phenol from the extract. DNA was precipitated
540 by incubation at –20°C overnight in 0.1 volume of 3 M Na-acetate (in MQ-water, autoclaved)
541 and 2.5 volumes absolute ethanol. Afterwards, the pellet was washed twice with 70% ethanol,
542 dried for 5 min, and re-suspended in 50 µL DNase- and RNAse- free H_2O. DNA concentrations
543 were quantified fluorimetrically using Quant-iT PicoGreen (Invitrogen).

544 **16S rRNA gene clone library**. Amplification of bacterial 16S rRNA genes was performed with
545 Bact8f (5'-AGA GTT TGA TYM TGG CTC-3') as forward primer (59) and 1492r (5'-N TAC
546 CTT GTT ACG ACT-3') as reverse primer (60). Archaeal species were targeted by AR109F
547 (5'-ACK GCT CAG TAA CAC GT-3') as forward (61) and AR915 (3'-GTG CTC CCC CGC CAA
548 TTC CT-3') as reverse primer (62). The PCR mixture contained 0.2 mM of each dNTP, 2 mM
549 $MgCL_2$, 20 µg BSA, 1 U of *Taq* DNA polymerase, and a Taq polymerase buffer with KCl
550 (ThermoFisher Scientific). The PCR was performed using an initial denaturation at 95°C for
551 5 min; 30 cycles of 95°C for 30 s, 50°C for 30 s, 72°C for 1.5 min; and a final elongation at
552 72°C for 7 min. For PCRs with archaeal primers, the annealing temperature was set to 55°C.
553 Amplification products were purified by use of the Zymo Research DNA Clean & Concentrator
554 Kit (Zymo Research). 16S rRNA clone libraries were obtained with the TOPO® TA Cloning®
555 Kit (ThermoFisher Scientific). Clones were screened by M13-PCR for inserts of the correct size

556 according to the manufacturer's instructions. Resulting PCR products of expected length were
557 purified by use of the Zymo Research DNA Clean & Concentrator Kit and sent for sequencing.

Supporting Tables

Table S1. Overview of inocula used to establish initial pyrite-forming enrichment cultures.

Enrichment	Date	Sampling area	Material	Medium†	Temp. (°C)	pH
J5*	Sept. 1995	Sewage treatment plant Konstanz, Germany	digested sewage sludge	freshwater	28	7.2
J2*	Sept. 1995	Sewage treatment plant Konstanz, Germany	digested sewage sludge	freshwater	16	7.2
J7	Apr. 1993	Rio Tentor (Venice, Italy)	brackish sediment	marine	16	7.2
J8*	Mar. 1991	Wadden sea sediment, Groningen, The Netherlands	marine sediment	marine	16	7.2
J9*	Apr. 1993	Fish market channel (Venice, Italy)	brackish sediment	marine	16	7.2
X1	Sept. 1995	Sewage treatment plant Tübingen-Lustnau, Germany	digested sewage sludge	freshwater	28	7.2
X2	Sept. 1995	Lake Constance, Güll	freshwater sediment	freshwater	28	7.2

† after Widdel and Pfennig (42)
* CH_4 formation observed

Table S2. Iron mineral analysis by Mössbauer spectroscopy at a temperature of 5 K in nearly 7-month-old (207 days) culture J5 incubated at various temperatures and in the presence of various inhibitors. Mössbauer parameters were obtained through Voigt based fitting (VBF). δ – isomer shift, ΔE_Q – quadrupole splitting, ε – quadrupole shift, B_{hf} – internal magnetic field, R.A. – relative area, X^2 – goodness of fit parameter. The absolute amount of formed FeS_2 was inferred from the relative area of the FeS_2 signal and the maximum amount of 350 µmol that could be produced if all FeS would have been converted to FeS_2.

Sample	Phase	δ (mm/s)	ΔE_Q (mm/s)	ε (mm/s)	B_{hf} (T)	R. A. %	X^2	FeS_2 (µmol)
Abiotic	FeS	0.43		0.15	13.1	64.3	1.67	
control	FeS_x	0.50	0.13			35.7		
4 °C	FeS	0.47	0.27			37.8	6.01	
	FeS_x	0.43		0.07	17.2	62.2		
16 °C	FeS_2	0.41	0.38			18.5	0.78	64.8
	FeS_x	0.39		0.02	19.2	48.8		
	FeS_x	0.42		–0.02	16.5	32.7		
28 °C	FeS_2	0.41	0.50			52.8	0.88	184.8†
Replicate I	FeS_x	0.32		0.07	15.7	38.9		
	Fe_3S_4	0.46		0.05	32.0	8.3		
28 °C	FeS_2	0.40	0.58			62.5	0.78	218.8§
Replicate II	FeS_x	0.29		–0.2	16.4	31.0		
	Fe_3S_4	0.60		–0.05	32.0	6.5		
46 °C	FeS_2	0.42	0.41			39.4	1.67	137.9
	FeS_x	0.10		–0.09	21.1	50.5		
	FeS_x	0.40		0.05	15.7	7.8		
	Fe_3S_4	0.64		0.03	33.2	2.3		
60 °C	FeS	0.54	0.16			27.1	1.74	
	FeS_x	0.34		0.05	2.4	21.6		
	FeS_x	0.55		–0.08	16.6	43.9		
	Fe_3S_4	0.63		–0.08	31.9	7.3		
Penicillin + 79% H_2	FeS	0.51	0.16			31.6	1.12	
(headspace)	FeS_x	0.38		0.15	5.3	17.4		
	FeS_x	0.85		0.01	23.0	37.5		
	FeS_x	0.46		–0.07	15.5	13.4		
Penicillin	FeS	0.46	0.27			26.4	1.15	
	Fe_3S_4	0.68		–0.04	33.1	8.8		
	Fe_3S_4	0.52		0.05	31.7	18.8		
	FeS_x	0.44		0.00	14.9	15.0		
	FeS_x	0.43		0.02	20.2	31.1		
BES	FeS	0.50	0.22			28.1	0.76	
	Fe_3S_4	0.69		–0.15	29.6	23.4		
	Fe_3S_4	0.62		0.02	33.1	7.1		
	FeS_x	0.25		0.15	7.4	20.2		
	FeS_x	0.44		–0.16	16.6	21.2		

† corresponding amount of formed CH_4: 44.9 µmol
§ corresponding amount of formed CH_4: 67.6 µmol

Supporting Figures

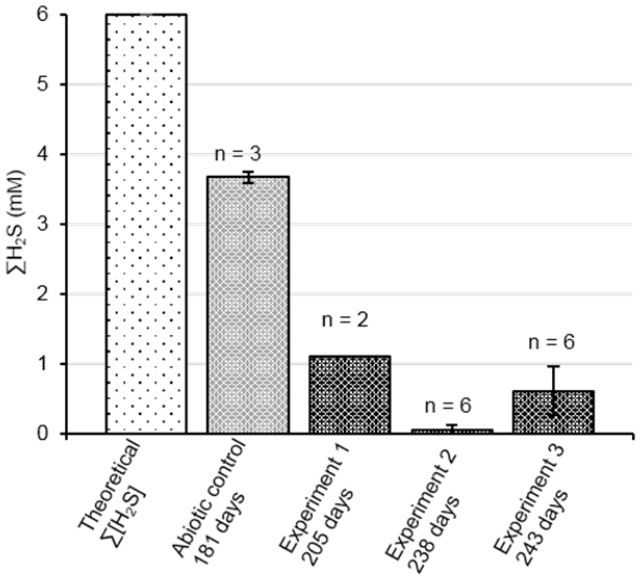

Figure S1. Total H_2S as the sum of $H_2S_{gaseous}$, $H_2S_{aqueous}$, HS^-, and S^{2-} in the non-inoculated medium as compared to the abiotic control and enrichment culture J5 in various independent incubation experiments. The time of incubation is indicated in days. Biological replicates are indicated as n.

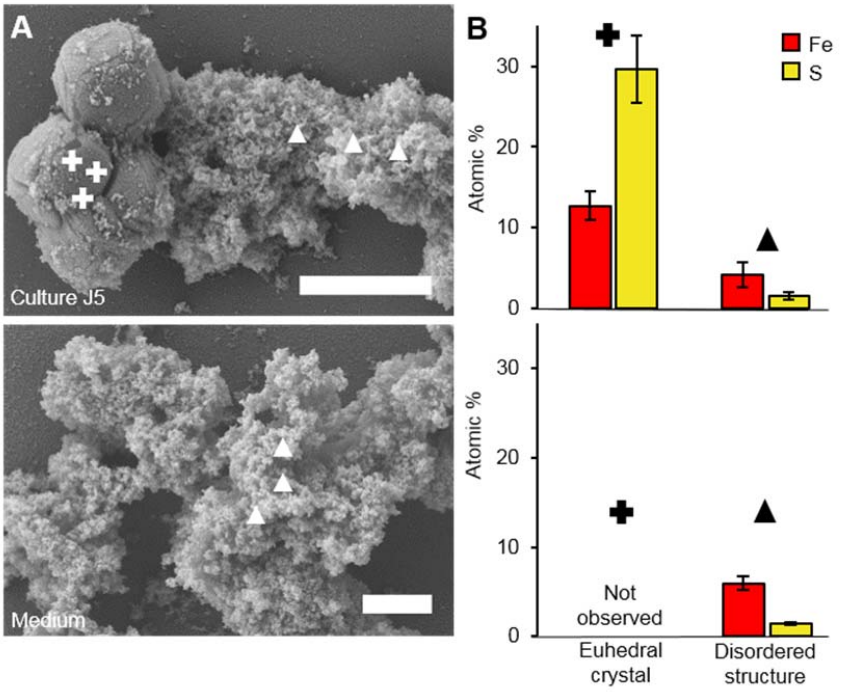

581

582 Figure S2. Fe:S ratio of different mineral phases in culture J5 and freshly prepared medium
583 without inoculum. (A) Exemplary scanning electron microscopy images used as guidance to
584 perform energy dispersive X-ray spectroscopy (EDX) point measurements of culture J5 after
585 nearly 10 months of incubation (295 days) and of freshly prepared medium without inoculum.
586 Scale bars represent 2 µm. Symbols in the SEM images indicate EDX point measurements
587 (crosses for crystals, triangles for disordered structure). (B) Atom percent ratio of iron (red) and
588 sulfur (yellow) as derived from EDX point measurements of euhedral crystals resembling pyrite
589 as well as disordered structures resembling the sum of the remaining Fe-S-mineral phase.
590 Measurements were done on eight different sampling areas with three EDX point
591 measurements each.

592

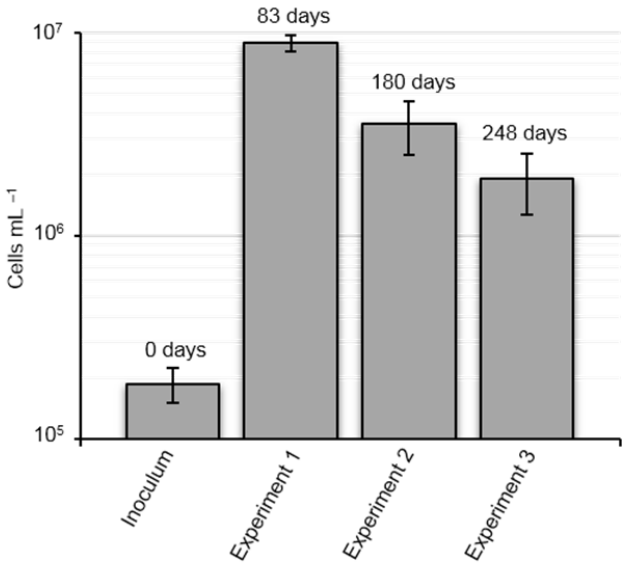

593

594 Figure S3. Average cell counts of culture J5 as based on DAPI-stained cells in three
595 independent incubation experiments at 28°C as compared to freshly inoculated medium. The
596 time of incubation is indicated in days. Data was obtained from biological duplicates, each
597 measured in technical triplicates. Standard deviations are given for technical replicates.

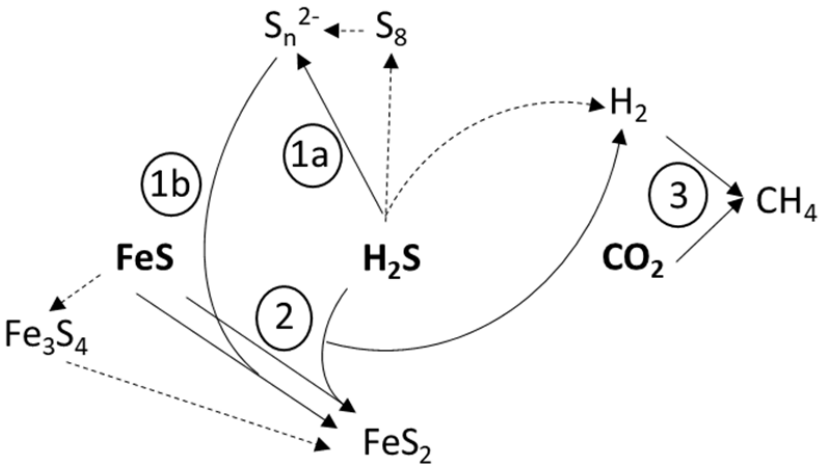

598

599 Figure S4. Schematic overview of potential FeS_2 formation pathways in culture J5. The
600 scheme illustrates pyrite formation either by a combination of sulfide oxidation to zero-valent
601 sulfur (1a) coupled to the polysulfide pathway (1b) or by the H_2S pathway (2). The released
602 reducing equivalents are likely transferred in the form of H_2 to methanogenesis (3) to reduce
603 CO_2 to CH_4. Dashed lines leading to *cyclo*-octasulfur (S_8) and greigite (Fe_3S_4) represent
604 potential alternative pathways or side reactions, respectively.